Comparative analysis of mammalian adaptive immune loci revealed spectacular divergence and common genetic patterns

Mariia Pospelova[1], Katalin Voss[2], Anton Zamyatin[1], Corey T. Watson[3], Klaus-Peter Koepfli[4], Anton Bankevich[1,5], Matt Pennell[2], Yana Safonova[1,5,*]

[1] Computer Science and Engineering Department, Pennsylvania State University, State College, PA, USA
[2] Department of Computational Biology, Cornell University, Ithaca, NY, USA
[3] Department of Biochemistry and Molecular Biology, University of Louisville School of Medicine, Louisville, KY, USA
[4] Smithsonian-Mason School of Conservation, George Mason University, Front Royal, VA, USA
[5] Huck Institutes of Life Science, Pennsylvania State University, State College, PA, USA
* Corresponding author: yana@psu.edu

Abstract

Adaptive immune responses are mediated by the production of adaptive immune receptors, antibodies and T-cell receptors, that bind antigens, thus causing their neutralization. Unlike other proteins, adaptive immune receptors are not fully encoded in the germline genome and result from a complex of somatic processes collectively called V(D)J recombination affecting germline immunoglobulin (IG) and T-cell receptor (TR) loci consisting of template genes. While various existing studies report extreme diversity of antibodies and T-cell receptors, little is known about the diversity of germline IG and TR loci. To overcome this gap, the first comparative analysis of full-length sequences of IG/TR loci across 44 mammalian species from 13 taxonomic orders was performed. First, germline genes counts were shown to correlate in IGH/IGL and TRA/TRB and anticorrelate in IGK/IGL, possibly indicating co-evolution between corresponding chains. Second, structures of IG/TR loci were analyzed, and it was shown that IG/TR loci formed by long arrays of high multiplicity repeats are more common for species that have experienced population bottlenecks. Finally, haplotypes of IG/TR loci with little or no sequence similarity within a species were found, suggesting that they may have a limited potential for homologous recombination. These results demonstrate that IG/TR loci are rapidly evolving genomic regions whose structural variation is shaped by the population history of the species and open new perspectives for immunogenomics studies.

Introduction

Adaptive immune responses are mediated by the production of antibodies (Abs) and T-cell receptors (TCRs) produced by B- and T-cells, respectively, that bind to bacteria, viruses, or aberrant cells (collectively called antigens) and cause their neutralization or destruction. The collection of expressed Abs (TCRs) in an individual is known as the Ab (TCR) repertoire. The

generation of diverse Abs and TCRs relies on a process called V(D)J recombination that somatically rearranges the DNA in individual B- and T-cells. In B-cells, this process affects germline *immunoglobulin* (*IG*) loci, in which individual IG genes including variable (V), diversity (D), and joining (J) genes are selected and generate a VDJ sequence corresponding to *the variable region* for either the heavy chain (HC) or the light chain (LC) of a given antibody (Tonegawa, 1983). Most mammalian genomes contain one IG heavy chain locus (IGH) and two immunoglobulin light chain loci: kappa (IGK) and lambda (IGL). Light chain loci do not contain D genes and generate VJ recombinations. In T-cells, the V(D)J recombination process affects germline *T-cell receptor* (*TR*) loci. Most mammalian species contain four types of TR loci: TR alpha (TRA), TR beta (TRB), TR gamma (TRG), and TR delta (TRD) loci encoding different types of TR chains. TRA and TRD loci contain V and J genes only, and TRB and TRG contain V, D, and J genes (Janeway et al., 2001).

While existing studies of adaptive immune repertoires note their extraordinary diversity resulting from V(D)J recombination (Alberts et al., 2022; Schroeder, 2006; Briney et al., 2019; Safonova et al., 2022), little is known about the structure of germline IG/TR loci encoding them. The main reason for this gap is high repetitiveness of IG/TR loci which makes them particularly difficult to reconstruct from short-read sequencing reads and often leads to fragmented assemblies (Watson et al., 2013; Rodriguez et al., 2020; Lin et al., 2024; Zhu et al., 2024). Since incomplete assemblies prevent a comprehensive analysis of germline sequences, comparative immunogenomics studies have instead focused on individual germline IG/TR genes (Ramesh et al., 2017; Luo et al., 2019; Kaduk et al., 2022; Sirupurapu et al., 2022; Pennell et al., 2023; Ma et al., 2024), which can still be identified in fragmented assemblies. These studies reported the remarkable sequence diversity of germline IG/TR genes across species, thus showing that the diversity of Ab/TCR repertoires is built upon it and is further enhanced by the somatic V(D)J recombination process.

Recent advances in long-read sequencing technologies and genome assembly methods have enabled nearly complete reconstruction of haplotype-resolved sequences of IG/TR loci, however, genetic characteristics and architecture of germline IG/TR loci remains poorly studied. Most existing comparative immunogenomics studies either focused on direct comparisons with human IG/TR loci (e.g., human and mouse IGH: Sepulveda et al., 2005; dog and human IGL: Martin et al., 2018) or studied a specific clade. For example, Rodriguez et al., 2023 analyzed germline human IGH loci and described novel structural variations across 150 individuals. Sampson and Miller, 2023 investigated the impact of mobile elements in marsupial IG loci. Yoo et al., 2024 characterized germline IG and TR loci of four great ape species and revealed that structural variations harbor specific-specific IG and TR genes. Pursell et al., 2024 analyzed bat IG loci and discovered an IGH locus duplication. Despite these advances, no study has conducted a broad comparative analysis of IG/TR loci across diverse clades. A major challenge lies in the rapid evolutionary divergence of these loci, which results in little to no sequence similarity across species. The inability to compute alignment and identify orthologous genes makes these regions difficult to analyze using comparative genomics tools such as IGV (Robinson et al., 2011) or SyRi (Goel et al., 2019) and raises a need in new approaches handling rapidly evolving regions.

In this paper, we attempted to close this gap and performed the first comparative study of full-length haplotype-resolved sequences of germline IG/TR loci across 44 therian mammalian species spanning 13 taxonomic orders. We combined the high-quality data generated from large-scale genome sequencing projects and developed a set of metrics describing germline gene diversity, haplotype divergence, and genomic architecture of IG/TR loci. We revealed associations between these metrics and found connections with species phenotypes.

Results

Predicting adaptive immune loci in mammalian assemblies. High-quality diploid genome assemblies of 44 therian mammalian species (42 placental and 2 marsupial mammals) representing 13 taxonomic orders were collected from the Vertebrate Genomes Project (Rhie et al., 2021; www.genomeark.org); the California Conservation Genomics Project (Shaffer et al., 2022; www.ccgproject.org), and the Bovine Pangenome Consortium (Smith et al., 2023; bovinepangenome.github.io) (**Fig. 1A**). For 3 out of 44 species (the cattle, the European badger, the black rhinoceros), parental information via trios was available and the genomes were haplotype phased; for one species (the brown bear), haplotypes were not separated; and for remaining 40 species, genomes were not phased, but both primary and alternate assemblies were available (**Table 1**). Each assembly except for that of the brown bear was marked with a haplotype label (primary/alternate; haplotype1/haplotype2; or maternal/paternal). To predict germline genes and determine the boundaries of IG/TR loci, the IgDetective tool (Sirupurapu et al., 2022) was modified to handle all types of adaptive immune loci and applied to the selected genomes (see "**Modifying IgDetective and filtering broken IG/TR loci**" in Methods). IG/TR genes were detected in both haplotype assemblies of each species, and, as a result, IGH, IGK, IGL, TRA, and TRB loci were predicted. TRG loci were predicted only for 9 species and were excluded from the analysis. TRA and TRD loci overlap and were not distinguished. The analysis was focused on V genes because they are easier to compare within and across species than D genes and are more numerous than J genes. We classified a V gene as productive if it was in-frame and did not contain internal stop codons. V genes that were detected by IgDetective but did not meet these criteria were classified as pseudogenes.

Adaptive immune loci can be distal. A *proximal* adaptive immune locus was defined as a sequence spanning V, D, and J genes, where adjacent genes are separated by no more than 300 kbp. Proximal loci with less than three productive V genes were classified as *orphans* and excluded from the analysis (**Table S1**). If germline genes of the same locus were still found in more than one contig in the assembly, the corresponding locus was considered broken during genome assembly. Several exceptions were made from this rule: 10 loci had several proximal regions located on the same contigs and separated by at least 300 kbp. For these cases, the locus boundaries were redefined based on the positions of the leftmost gene in the leftmost proximal locus and the rightmost gene in the rightmost proximal locus, and the locus was reclassified as *distal*. Previously identified distal IGK loci were reported in humans and gorillas, and distal IGL loci were found in bonobo (Lefranc, 2001; Engelbrecht et al., 2024; Yoo et al., 2024). **Fig. 1A** shows that distal loci emerge across different branches of the mammal evolutionary tree. **Fig. S1** showing dot plots of 10 distal IG/TR loci illustrates that long-range

inversions likely played a role in the formation of five of them (the Chinese pangolin IGK, the European snow vole TRA, the nine-banded armadillo IGK, the slow loris IGL, the tammar wallaby IGK), and the mechanisms underlying the formation other five distal loci (the deer mouse IGL, the European snow vole IGK, the gray short-tailed opossum IGL, the nine-banded armadillo IGH, the tammar wallaby IGL) are less unclear. The number of proximal regions per distal locus varies from 2 to 13 (**Fig. 1B**), and the lengths of non-coding regions between them vary from 300 to 3677 kbp (**Fig. S1**). On average, distal adaptive immune loci are longer than the proximal ones (Kruskal-Wallis test, $P=6.82\times10^{-7}$, **Fig. 1C**) and encode more V genes (Kruskal-Wallis test, P=0.02, **Fig. 1D**). It is unclear whether all proximal parts of a distal IG/TR locus can participate in V(D)J recombination, however, the fact that they were detected across different taxonomic orders suggests that it is a relatively common phenomena that might contribute to expansion of IG/TR loci. Population-wide genome sequencing data and data from expressed adaptive immune repertoires will help to better understand frequency and functionality of distal IG/TR loci.

Co-evolution of IG and TCR chains are associated with V gene counts. In total, the number of species with at least one fully assembled locus (both proximal and distal) varies from 36 to 43 across five types of immune loci (**Fig. 1A**). The number of species with two fully assembled and phased immune loci (both proximal and distal) varies from 18 to 21 for IGH, IGK, IGL, TRA loci and equals 33 for TRB loci (**Fig. 1A**). These numbers enable comparative analyses and suggest that the assembly complexity is comparable across all five types of adaptive immune loci. IGK loci were not detected in the five Chiroptera species, which is consistent with previous results (Pursell et al., 2024). Similarly, 2 out of 6 Rodentia species (the Merriam's kangaroo rat, the Botta's pocket gopher) did not have IGL loci, which is also consistent with previous studies describing short IGL loci in mice (Kos et al., 2022).

For all intact and proximal IG/TR loci, counts of productive V genes were compared. For Chiroptera species without IGK loci and Rodentia species without IGL loci, zero V genes were specified. **Fig. 1A** shows that the number of V genes per locus varies greatly across the species. The largest number of productive V genes was found in the brown big-eared bat IGH (640 V genes), the northern bat IGH (246 V genes), and the European snow vole IGH (217 V genes). All other loci contain less than 200 productive V genes. Counts of V genes positively correlate (all P-values < 0.01) with lengths of corresponding loci across all chain types (**Fig. S2A**).

Association analysis revealed links between V gene counts across some pairs of chains. First, counts of IGHV and IGLV genes positively correlate (here and further Pearson's correlation is used, r=0.44, P=0.007; **Fig. 2A**). To assess whether the relationships between different chains and loci remains significant after accounting for shared evolutionary history, a phylogenetic linear model implemented in the *phylolm* package (Lam et al., 2014) with the lambda model (Freckleton et al., 2002) was used. Prior to the analysis, all values were log-transformed to ensure model fit. The detected correlation holds true after accounting for phylogenetic autocorrelation among the analyzed species (lambda=1, P=0.07). This result suggests that IGH and IGL loci co-evolve either in the response to one another, or in a shared genetic environment. While a similar relationship between IGH and IGK loci was not observed (**Fig. S2B**), the total IG light chain V gene (IGKV+IGLV) counts have a higher correlation with IGHV gene counts as compared to IGH/IGL

(r=0.51, P=0.003, **Fig. S2C**). Counts of IGKV and IGLV genes show a stronger anticorrelation (r=–0.59, P=0.0003; **Fig. 2B**). This relationship was no longer significant when the slope was estimated with a phylogenetic regression (P=0.17), but the phylogenetic distribution of the counts appears discordant with the assumptions of phylogenetic regression (Uyeda et al., 2018) so we do not feel confident in the latter approach. We hypothesize that IGK and IGL chains play different roles across species, and expansion of one light chain locus leads to eventual contraction of another light chain locus. We also observed positive correlations between TRAV and TRBV gene counts (r=0.70, P=1.46×10^{-6}; **Fig. 2C**). This observation holds after accounting for phylogenetic autocorrelation (lambda=1, P=0.01). Because TRA and TRB loci encode α and β chains of the T-cell receptor, respectively, we assume that these loci co-evolve similarly to IGH/IGL loci.

IG loci diverge faster than TR loci, and IGH loci diverge the fastest. To compare two sequences S_1 and S_2 representing loci of the same type of IG/TR loci, a new *locus distance* metric was introduced. First, local alignments between S_1 and S_2 using the YASS tool (Noé and Kucherov, 2005) were computed. Alignments longer than 5 kbp were analyzed, and the percentage of each of the sequences covered by these alignments was computed. The *locus similarity* of S_1 and S_2 was computed as the average of the corresponding fractions, and the *locus distance* was computed as 100 – the locus similarity. For each pair of loci of the same chain type, the distance between corresponding species was also calculated using the TimeTree5 database (Hedges et al., 2015). As expected, species distances positively correlate with locus distances for all IG and TR loci (r=0.81, P=<0.0001, **Fig. 3A, Fig. S3**); however, the locus distance values were distributed unevenly. Analysis of locus distances for the same species distances showed that IG loci were more diverged compared to TR loci (Kruskal-Wallis test, P=0.005); and IGH loci were the most diverged (Kruskal-Wallis test, P(IGH, IGK)=0.03, P(IGH, IGL)=1.22×10^{-7}) (**Fig. 3B**). This suggests that IG loci evolve more rapidly and have fewer evolutionary constraints compared to TR loci. This might be explained by specifics of antigen recognition of antibodies and T-cell receptors: while antibodies bind antigens directly, TCRs also need to recognize the major histocompatibility complex representing antigen on the cell surface. Similarly, the faster divergence of IGH loci compared to IGK and IGL loci may reflect their distinct roles in antibody repertoires and respective evolutionary pressures. Previous studies report that IGH loci harbor more diverse V genes in primates (Yoo et al., 2024) and mice (Kos et al., 2022) and hypothesize that their primary role in antibody repertoires is to generate VDJ recombination diversity, while IGK and IGL chains protect against self-reactivity and maintain antibody stability (Collins and Watson, 2018).

Some IG/TR loci are formed by high multiplicity repeats. Even though the direct comparison of IG/TR loci across species is often not possible, analysis of their genomic sequences allowed us to reveal their common features. Previous studies have shown that some IG/TR loci consist of large arrays of multiplicity repeats (e.g., the cattle IGH locus by Li et al., 2023), while others have local areas with repeat expansions (e.g., IGH loci of human and mouse, Sepulveda et al., 2005; IGH loci of great apes, Yoo et al., 2024) or are not repetitive at all (e.g., TRA loci of great apes, Yoo et al., 2024). To distinguish between these cases, the *high multiplicity repeat content (HMRC)* metric was developed and computed for each locus *S* as the fraction of positions in *S* covered by repeats of length at least *L* at least *N* times. Positions of repeats were computed as boundaries

of the local alignments computed by YASS while aligning the locus versus itself. By default, *L*=15 kbp and *N*=5 (see "**Computing high multiplicity repeat content of IG/TR loci**" in Methods). The computed HMRC values were binned into three classes: high (HMRC: 0.6–1), medium (HMRC: 0.1–0.6), and low (HMRC: 0–0.1). Boundaries between classes were determined according to the largest relative drops of values in the sorted HMRC list. IG loci have higher HMRC compared to TR loci and IGH loci have the highest HMRC values (**Fig. 3C & Fig. 3D**). HMRC was not associated with V gene counts (**Fig. S4A**) nor locus lengths (**Fig. S4B**).

IG/TR loci formed by high multiplicity repeats have a lower V gene diversity. To reveal features associated with repetitiveness, V gene similarities were analyzed. First, for each productive V gene, the closest V gene match within the same locus and the corresponding percent identity were computed. Then the average value of the best percent identities (*average percent identity*) was computed for each locus. The average percent identity is higher in IG compared to TR loci (Kruskal-Wallis test, P<0.0001; **Fig. S5**) and higher in IG/TR loci with high HMRC (95.1%) as compared to IG/TR loci with medium (92%) and low (80.2%) HMRC (Kruskal-Wallis test, $P=3.06\times10^{-9}$). This suggests that IG/TR loci with high HMRC harbor genes residing in copies of the repeat units (**Fig. 3E**). Moreover, IG/TR loci with high HMRC have a higher percentage of V genes with >95% similarity to another V gene within the same locus (average 61.0%) compared to IG/TR loci with medium (45.8%) and low (18.4%) HMRC (Kruskal-Wallis test, $P=3.05\times10^{-9}$, **Fig. 3F**). Both figures have a descending trend suggesting that coverage by high multiplicity repeats is an important factor contributing to V gene similarity. Visual analysis of examples of IG/TR loci with high HMRC shows that V genes reside in recent repeat units (**Fig. 3G,** the top line). In IG/TR loci with medium HMRC, units of repeats are either more diverged or cover a smaller fraction of the locus sequence thus resulting in V genes with lower similarity (**Fig. 3G**, the middle line). In IG/TR loci with low HMRC, IG genes do not belong to repeat copies and are potentially more likely to be dissimilar (**Fig. 3G**, the bottom line).

IG/TR loci formed by high multiplicity repeats have a higher coverage by mobile elements. To reveal possible factors leading to high HMRC in IG/TR loci, the known classes of repeats were also computed using RepeatMasker (Chen et al., 2004). For each repeat type and each IG/TR locus, the percentage of the locus positions covered by repeats of a certain type was computed. The most abundant repeat classes are LINE/L1 (average locus coverage 18.8%), LTR/ERVL (1.9%), simple repeats (1.8%), LTR/ERVL-MalR (1.3%), LTR/ERV1 (0.9%), and low complexity sequences (0.5%) (**Fig. 4A**). Three types of know repeats revealed associations with HMRC: IG/TR loci with high HMRC have higher coverage by LINE/L1 (Kruskal-Wallis test, P=0.01) and LTR/ERV1 repeats (Kruskal-Wallis test, P=0.001) and lower coverage by low complexity regions (Kruskal-Wallis test, P=0.005) compared to IG/TR loci with low and medium HMRC (**Fig. 4B & 4C, Fig. S6**). These associations suggest that mobile elements might play a role in the formation of high IG/TR loci.

IG/TR loci with high HMRC are common for species that have undergone past population bottlenecks. Previous studies of plant genomes revealed elevated frequency of mobile element movements in inbred populations (Chen et al., 2020; De Kort et al., 2022). These studies suggest that inbreeding increases the fraction of recessive mutations and break mechanisms silencing

mobile elements thus leading to structural diversification of the genome. To explore similar connections between IG/TR loci with high HMRC and population dynamics of the observed species, the effective population size (N_e) was computed for each analyzed species using a modification of the PSMC model (Li & Durbin, 2011; see "**Computing the effective population size**" in Methods). For each species, N_e values were computed over a period of time, and population bottlenecks were computed as local minimums of the N_e curve and detected for 42 out of 44 species. We only considered past bottlenecks and used the T_{min} threshold (by default, T_{min}=50,000 years ago) for discarding bottlenecks occurring after it. The choice of T_{min} is discussed in "**Selecting a threshold for filtering out recent population bottlenecks**" in Methods. For each species, the lowest N_e value during a population bottleneck was identified. Because HMRC varies across loci with a species and previous studies suggested that structural diversification is a genome-wide effect, the maximum HMRC value and the corresponding HMRC class were selected across all five types of IG/TR loci for each species (**Fig. 4D**; **Table 2**). Species which IG/TR loci have high HMRC went through more severe bottlenecks with the average minimum N_e 8598 as compared to species which IG/TR loci have medium and low HMRC with an average minimum N_e of 14,123 (**Fig. S7**). To account for the impact of closely related species, two groups of species with similar loci were identified: IGH loci of felines (the clouded leopard, mountain lion, bobcat, and Canada lynx) and IGH loci of cetaceans (the vaquita and minke whale) (**Table 2**; **Fig. S8**). To minimize the impact of these groups, the average HMRC and the minimum N_e at the bottleneck were computed for each of two groups; the HMRC class was assigned according to the binning in **Fig. 3C**. No pair of IG/TR loci had sufficient sequence similarity after collapsing these two groups. For the collapsed species, the observed pattern holds true with a P-value 0.04 (Mann-Whitney U test) (**Fig. 4E**). We suggest that mobile element movements increased during inbreeding have a pronounced influence on rapidly evolving IG and TR loci, leading to their structural diversification. While structural variations driven by mobile elements are often either neutral or deleterious at the genome-wide level (Solyom et al., 2012; Consuegra et al., 2021), this process may increase the genetic diversity of IG/TR loci through the generation of new gene-carrying repeat copies in populations suffering from losses of heterozygosity (**Fig. 4F**).

IG loci accumulate more variations within a population compared to TR loci. To study the variation of IG/TR loci within a population even further, within each species and locus, we collected all pairs of homologous haplotype-resolved loci. Pairs of sequences where one locus is under assembled were discarded (see **"Detecting under assembled haplotype-resolved IG/TR loci"** in Methods). As a result, 95 haplotype-resolved pairs of IG/TR loci including 19 IGH, 15 IGK, 14 IGL, 20 TRA, and 27 TRB haplotypes were analyzed. To describe the level of variation between pairs of homologous haplotypes, *the haplotype similarity* metric was developed and employed. First, for each pair of haplotypes, local alignments were computed using YASS and sorted in descending order based on their lengths. For each haplotype in the pair, the sequence fraction covered by n longest alignments was computed for all n ranging from 1 to the total number of reported alignments (by default, n = 100). Computed fractions form a curve $F(n)$, where n is the number of longest alignments. While the $F(n)$ curves of similar haplotypes are expected to match (**Fig. S9A**), the $F(n)$ curves of dissimilar haplotypes will have different shapes and areas under the curve (**Fig. S9B**). For each haplotype pair, the areas under two $F(n)$ curves (A_1 and A_2) and the area between the curves (A_{12}) were computed. Then A_{12} was subtracted from the average of

A_1 and A_2, and the resulting value was referred to as the *haplotype similarity*. Because the maximum area under each curve is 100, haplotype similarity values vary from 0 (for diverged haplotypes) to 100 (for identical haplotypes). 95 haplotype pairs have haplotype similarity ranging from 21 to 100 (**Fig. 5A**), and TR haplotypes are more similar compared to IG haplotypes (Kruskal-Wallis test, $P=2.7\times10^{-3}$; **Fig. 5B**). IG haplotype similarity has a higher variance, which could be partially explained by the contribution of four taxonomic orders: the analyzed Artiodactyla and Carnivora species have more similar IG locus haplotypes compared to Chiroptera and Rodentia species (Kruskal-Wallis test, $P=1.33\times10^{-6}$; **Fig. 5C**). This pattern persists in TR pairs (Kruskal-Wallis test, $P=7.81\times10^{-4}$); however, haplotype similarity values are less distinct (**Fig. S10**). **Fig. 5D** showed that, within Chiroptera and Rodentia orders, diverged haplotypes can be completely dissimilar (e.g., the Townsend's big-eared bat IGH) or characterized by dissimilar islands connected by more conserved fragments (e.g., the California vole IGH).

Diverged IG haplotypes might be subject to limited homologous recombination. For each productive V gene in a haplotype pair, the closest V gene in another haplotype and the corresponding percent identity of the alignment were computed. Only IG haplotypes were analyzed because of the higher variance of haplotype similarity values. For each haplotype-resolved IG locus, the average percent identity of V genes collected across both haplotypes was computed. The computed V gene similarities positively correlated with haplotype similarity values ($r=0.79$; $P=1.59\times10^{-11}$; **Fig. 5E**). **Fig. 5E** shows two outliers in the lower left corner (low gene similarity; low haplotype similarity), exclusion of which did not significantly change the correlation value ($r=0.76$, $P=8.57\times10^{-10}$). To reveal pairs of homologous V genes in each haplotype pair, the computed pairwise distances of V genes were combined into a distance matrix. The hierarchical clustering followed by flattening the dendrogram and extraction of clusters at the same cophenetic distance were applied to the matrix. The distance threshold was selected to maximize the number of clusters of size two. A cluster of size two was classified as homologous if it consisted of V genes from different haplotypes. The percentage of homologous pairs positively correlates with haplotype similarity ($r=0.61$, $P=4.05\times10^{-6}$; **Fig. 5F**). We also computed the percentage of clusters of size two where one V gene is productive and another is pseudogene and showed that it negatively correlates with haplotype similarity ($r=-0.46$, $P=0.001$; **Fig. 5G**). Correlations shown in **Fig. 5F, 5G** and the lack of homology between highly diverged IG haplotypes suggest that they might be excluded from chromosomal crossovers and inherited as one continuous allele (**Fig. 5H**). This possibly leads to an increase of V gene diversity, a decrease of homologous V gene pairs, an accumulation of V genes with broken copies. While mechanisms leading to the emergence of highly diverged IG haplotypes are unknown, we hypothesize that introgression (Zhang et al., 2016), suppressed recombination (Todesco et al., 2020), and / or elevated mutation rates (Xie et al., 2019) could play a role in their formation.

Discussion

In this paper, five types of IG/TR loci (IGH, IGK IGL, TRA, and TRB) of 44 mammalian species across 13 taxonomic orders were characterized and compared. First, germline IG/TR genes were detected, and the gene counts across all pairs of IG/TR loci were compared. V gene counts in IGH and IGL loci showed a strong positive correlation suggesting that V genes of IGH and IGL

loci may have evolved to generate preferential or more optimal pairs of heavy and light chain genes within expressed antibodies. A similar observation was made for TRA and TRB loci. These observations align with previous reports of preferential chain pairings in Abs and TCRs (DeKosky et al., 2016; Banach et al., 2021; Jaffe et al., 2022; Raybould et al., 2024) and might be important in future monoclonal antibody and TCR design studies.

On the contrary, V gene counts in IGK and IGL loci have a negative correlation, suggesting that the expansion of one locus leads to the contraction of another locus. These findings imply that immunoglobulin light chain loci serve different roles in B cell development and antigen recognition across mammalian species. For example, while human IGK locus is generally rearranged first, and IGL locus is rearranged if the IGK chain generates a non-productive or self-reactive rearrangement (Collins and Watson, 2018); IGL locus generates the majority of the initial antibody repertoire in pigs (Wertz et al., 2013). Follow-up studies of IGH, IGK, and IGL chain roles in mammalian antibodies will require expressed antibody repertoire sequencing data with paired chains (e.g., scRNA-Seq) and will be important for understanding the mechanisms of mitigating self-tolerance in antibodies and B-cell development across various species.

Pairwise analysis of IG/TR locus sequences shows that they evolve rapidly, which makes comparative analysis of their sequences through alignments difficult. Despite high sequence variability, some IG/TR loci share common organizational patterns. We observed that certain IG/TR loci consist of high multiplicity repeats, although the specific repeat units vary across species. Such IG/TR loci have a higher coverage by mobile elements and are more commonly found among species that went through severe population bottlenecks compared to non-repetitive IG/TR loci. This observation aligns with previous studies showing that inbreeding caused by population bottlenecks leads to activation of mobile elements and eventual structural diversification of the genome (Chen et al., 2020; De Kort et al., 2022) and suggests that a similar process takes place in inbred mammalian populations. Unlike other types of structural variations, high-multiplicity repeats can be detected using one locus sequence per species, and it is unclear whether other structural variations are associated with population bottlenecks. Generating population-wide genomics data across different species will be crucial for uncovering these evolutionary relationships.

IG/TR loci with high values of high multiplicity repeat content are characterized by a lower diversity of germline V genes because they reside in repeat copies. While a high diversity of germline genes is generally considered beneficial for boosting the diversity of naive adaptive immune repertoires (Bratsch et al., 2011; Schountz et al., 2017; Pennell et al., 2023), there is insufficient evidence to conclude that species with highly repetitive IG/TR loci have a reduced capacity to generate diverse immune responses. Further studies on expressed antibody and TCR repertoires are needed to address this question. Existing studies suggest that some species may have a higher diversity of D and J genes or evolved compensatory diversification mechanisms, such as ultralong cysteine-rich antibodies in bovines (Wang et al., 2013). Identifying similar mechanisms in other species could provide insight into the role of germline IG/TR diversity in shaping immune system versatility. If the germline diversity is shown to be a critical factor, it raises serious

concerns as many species today are experiencing population declines due to human-induced habitat loss and fragmentation, potentially threatening the robustness of their immune systems.

Finally, analysis of haplotype-resolved IG/TR loci showed that some haplotypes do not share visible sequence similarity. Such loci are more prevalent in rodents and bats, and the mechanisms of their formation are unknown. Previously low sequence similarity of IG/TR loci and genes was reported for zoo animals (e.g., the Philippine flying lemur in Zhu et al., 2024) and model organisms (e.g., the mouse IGH, Watson et al., 2019; the macaque IGH, Peres et al., 2025) and suggests that human-mediated subpopulation mixing may be a contributing factor. Our analysis further showed that dissimilar haplotypes, while exhibiting high V gene diversity, also contain a higher proportion of broken V gene copies, suggesting that these loci may be partially or completely excluded from crossover events and thus accumulate pseudogenes at a faster rate. In this model, the entire IG/TR locus haplotype functions as a single continuous allele with a higher degree of linked polymorphisms. This observation raises important challenges for the development of IG/TR nomenclature in model organisms and opens new genomic questions. Specifically, it remains unclear how adaptive immune responses differ between species with highly diverged versus highly similar IG/TR haplotypes. Taking into account that conservation management strategies often involve subpopulation mixing, this question is particularly relevant to understanding how recovered populations adapt to wild environments.

In summary, IG/TR loci provide a unique perspective on genomic sequence diversity. Das et al., 2012 hypothesized that adaptive immune loci might have fewer evolutionary constraints due to V(D)J recombination. We expand on this idea, proposing that these regions are also highly susceptible to structural diversification, making them an ideal model for studying structural variations and answering important questions in fundamental and applied genomics. Further research on IG/TR loci and expressed adaptive immune repertoires both across and within populations will be essential for addressing these challenges and uncovering new insights into immune system evolution and function.

Methods

Modifying IgDetective and filtering broken IG/TR loci. The original version of IgDetective developed by Sirupurapu et al., 2022 was modified to detect both IG and TR V, D, J genes and determine boundaries of the respective loci. In addition to the RSS-based search described in the original work, we implemented an iterative procedure that aligns previously detected V genes to the input genome using minimap2 (Li., 2018) until no new V genes are detected. Groups of IG/TR genes separated by no more than 300 kbp were reported as IG/TR loci, and loci consisting of less than 10 V genes were discarded to filter out orphan genes. Boundaries of a locus were determined as 10 kbp before the leftmost IG/TR gene and 10 kbp after the rightmost position IG/TR gene. Loci with more than one contig per haplotype were discarded as under-assembled (**Table S1**). The only exception was made for bat species that have duplicated IGH loci (Pursell et al., 2024). Both copies of IGH loci were used for the analysis, and pairs of homologous IGH locus copies were found for the haplotype analysis.

Computing high multiplicity repeat content of IG/TR loci. Because structural organization of the analyzed IG/TR loci is highly variable from species to species (and even within the same species), we computed a set of relaxed metrics $R(L, N)$ showing the fractions of input sequence positions covered by repeats of length at least L at least N times. Such metrics allowed us to account for various types of segmental duplications and diverged repeat copies. L={10000, 15000} and N={3, 5} were tested and demonstrated high positive correlations with each other (**Fig. S11**). We thus used the strictest combination for the downstream analysis $R(15000, 5)$. Further increasing L and N values resulted in zero values of $R(L, N)$ for most loci and were discarded as non-informative.

Computing the effective population size. The Pairwise Sequentially Markovian Coalescent (PSMC) model (Li and Durbin, 2011) was utilized to infer effective population size (N_e) history for each mammalian genome assembly. The PSMC model is a widely adopted computational approach for demographic inference from a single genome. It analyzes the frequency of heterozygous sites throughout the genome to reconstruct the historical population size dynamics. Typically, heterozygous sites are identified by aligning short-read whole-genome sequencing data to a haploid genome assembly. However, modern Vertebrate Genomes Project (VGP) genome assembly pipelines (Rhie et al., 2021) primarily rely on PacBio HiFi sequencing, and Illumina short reads are not always produced. With haplotype-resolved genome assemblies, it is possible to directly identify all genetic differences between haplomes. To simplify the pipeline and leverage existing PSMC-compatible tools, we instead simulated perfect Illumina-like reads from the complete diploid genome assembly, employing a uniform coverage model with 10x coverage and a read length of 150 bp, these parameters were chosen to ensure compatibility and reliable performance of the existing tools. Subsequently, we followed the pipeline described by Li and Durbin, 2011: we aligned the simulated reads to either the primary haplotype or haplotype1, depending on the assembly curation, using BWA-MEM (Li, 2013). From these sorted alignments, we generated consensus sequences in FASTQ format using samtools (Danecek et al., 2021), capturing heterozygous positions between the two haplotypes through ambiguous nucleotide notation. The consensus FASTQ file was then processed using the internal PSMC utilities to generate the binary sequence input required for the PSMC analysis. Finally, we performed the PSMC analysis using the default parameters recommended by the developers. This pipeline efficiently enables the direct application of the PSMC model to diploid genome assemblies, eliminating the necessity for additional short-read sequencing data. To scale the PSMC trajectories, we applied parameters originally estimated for humans: a uniform mutation rate of 2.5×10^{-8} mutations per site per generation and a generation time of 25 years. These values were used consistently across all species in our study. We acknowledge that species-specific mutation rates and generation times would yield more accurate time scaling and absolute N_e estimates. However, due to the lack of reliable estimates for many of the analyzed species, we opted to use uniform parameters to facilitate consistent comparative purposes.

Selecting a threshold for filtering out recent population bottlenecks. The Ne curves were computed in the time frame from 0 to 27M years ago. To identify the minimum T_{min} threshold, we tested values starting from 10,000 to 200,000. For all T_{min} values, species with IG/TR loci with the high HMRC have lower minimum Ne at bottlenecks compared to the medium and high classes

470 (**Fig. S12).** We thus selected the first value (T_{min} = 50,000) resulting in a statistically significant
471 association.
472
473 **Detecting under assembled haplotype-resolved IG/TR loci.** Visual assessment of dot plots
474 computed for IG/TR haplotypes revealed that some pairs represent potentially broken assemblies
475 even if each haplotype has only one contig for the corresponding IG/TR locus. In most cases, we
476 were able to make this conclusion because a noticeable part of the prefix or suffix of one of the
477 contigs in the pair was not aligned to another contig in the pair (**Fig. S13**). Because the described
478 haplotype similarity metric will be artificially low in such cases, we excluded such pairs from the
479 analysis. In total, 20 out of 115 haplotype pairs were excluded from the analysis using this
480 procedure.

481 Contributions

482 MPo, CWT, KPK, MPe, and YS conceptualized the study. MPo, KV, AZ, AB, MPe, and YS
483 designed experiments and performed computational analyses. MPo and YS wrote the manuscript.
484 All authors have approved the text and provided comments to it.

485 Conflict of interests

486 We declare no conflict of interest.

487 Data availability

488 The new version of IgDetective is publicly available at GitHib:
489 github.com/Immunotools/IgDetective. Scripts and computed characteristics of species and loci
490 (N_e statistics, locus lengths, gene counts, similarity metrics) are available at
491 github.com/posma/ComparativeImmunogenomics.

Figures

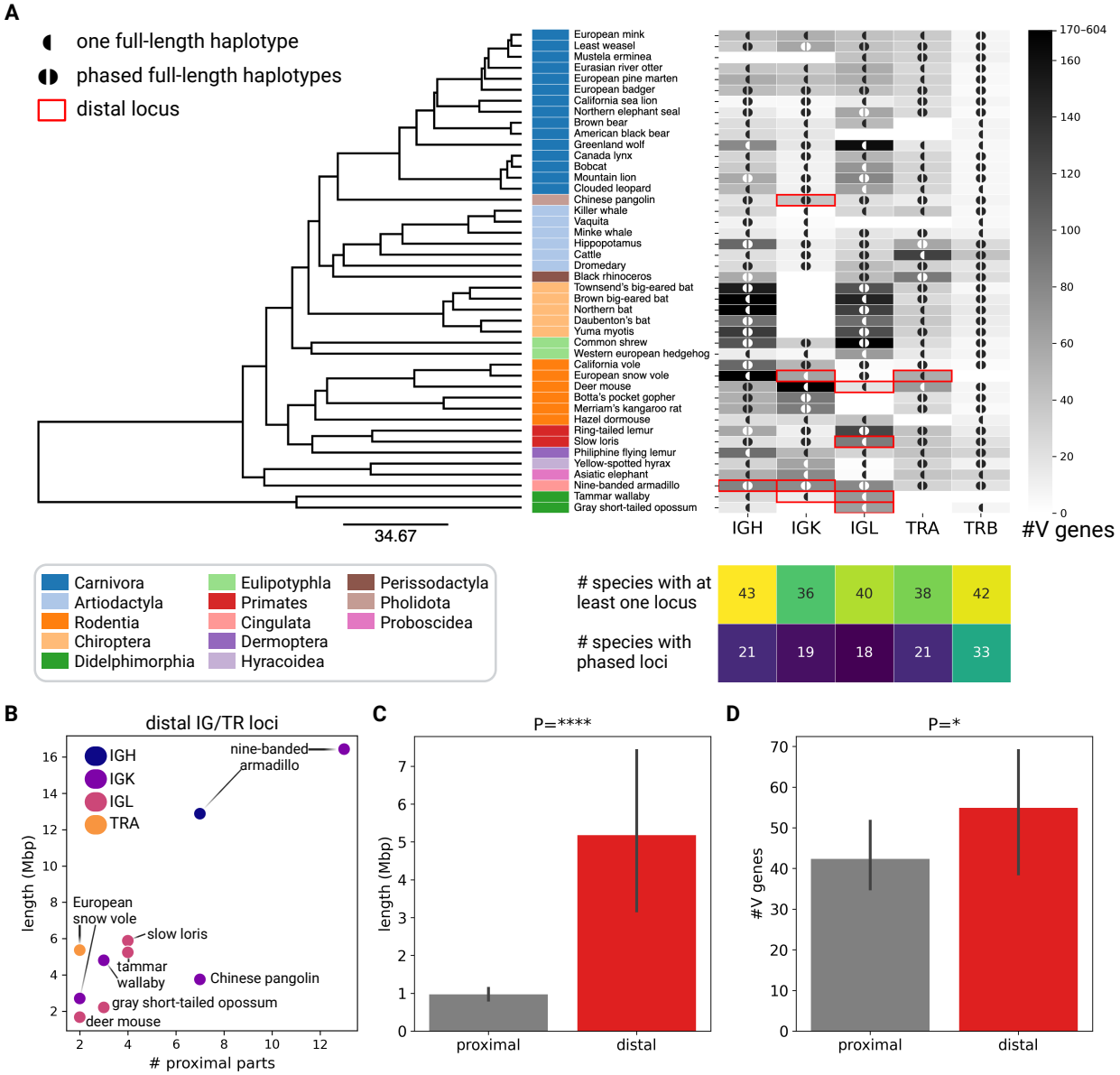

Figure 1. Overview of IG/TR loci collected across 44 mammalian species. (A) The phylogenetic tree of mammalian species selected for the analysis. The tree was constructed using consensus topologies derived from 100 trees obtained from VertLife.org (Upham et al., 2019). The final consensus tree was generated with TreeAnnotator v1.10.4 (Drummond et al., 2007) using mean node heights. Taxonomic orders are color coded and shown next to the species names. Counts of productive V genes in IGH, IGK, IGL, TRA, and TRB loci are shown on the heatmap on the right. Distal IG/TR loci are shown as red rectangles. A locus is marked with ◖ /◖ ◗ if it has one/two intact haplotype(s) assembled. Counts of such sequences are summarized in the heatmap below. **(B)** Number of proximal parts vs the total locus length across 10 distal IG/TR loci. **(C)** Lengths of proximal and distal IG/TR loci. Here and further error-bars represent 95%

504 confidence intervals; P-values are denoted as follows: ns: P≥0.05; *<0.05, **<0.01, ***<0.001,
505 ****<0.0001; and P-values are computed using the Kruskal-Wallis test unless specified otherwise.
506 **(D)** Counts of productive V genes in proximal and distal IG/TR loci.

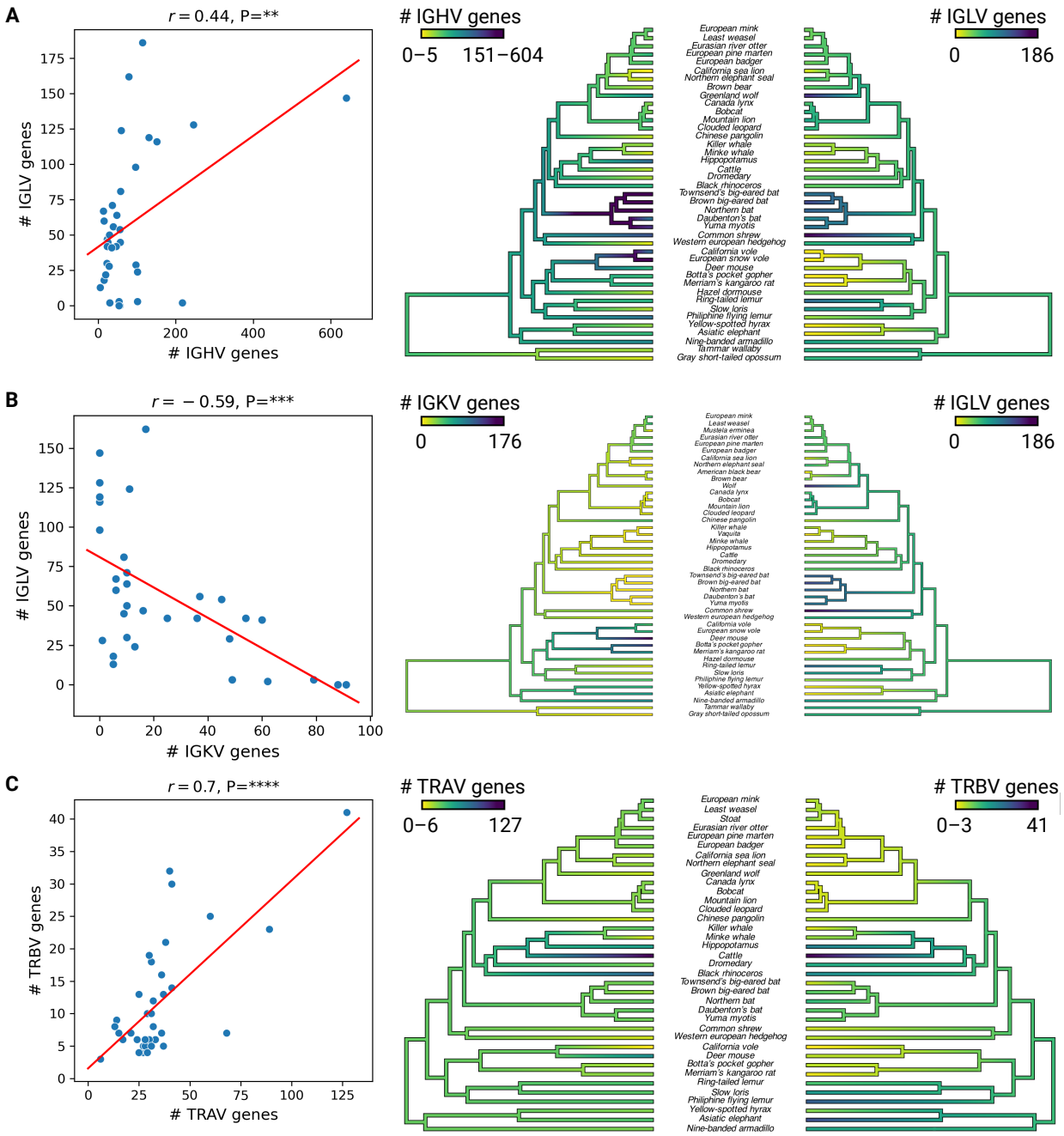

Figure 2. Correlations between productive V gene counts in proximal IG/TR loci. (A) Counts of IGHV and IGLV genes across 36 species. Only species with at least one reconstructed IGH locus and at least one reconstructed IGL locus were chosen. The Pearson's correlation and the corresponding P-value are shown at the top of the plot. The red line shows the linear trend. The trees on the right show the species tree colored according to IGHV and IGLV gene counts, from yellow (0) to blue (the maximum V gene number). The species tree from **Fig. 1** was used and the gene counts visualized with the contMap function from the phytools R package (Revell, 2024). **(B)** Counts of IGKV and IGLV genes across 32 species. **(C)** Counts of TRAV and TRBV genes across 37 species. Legends of (B) and (C) are consistent with (A).

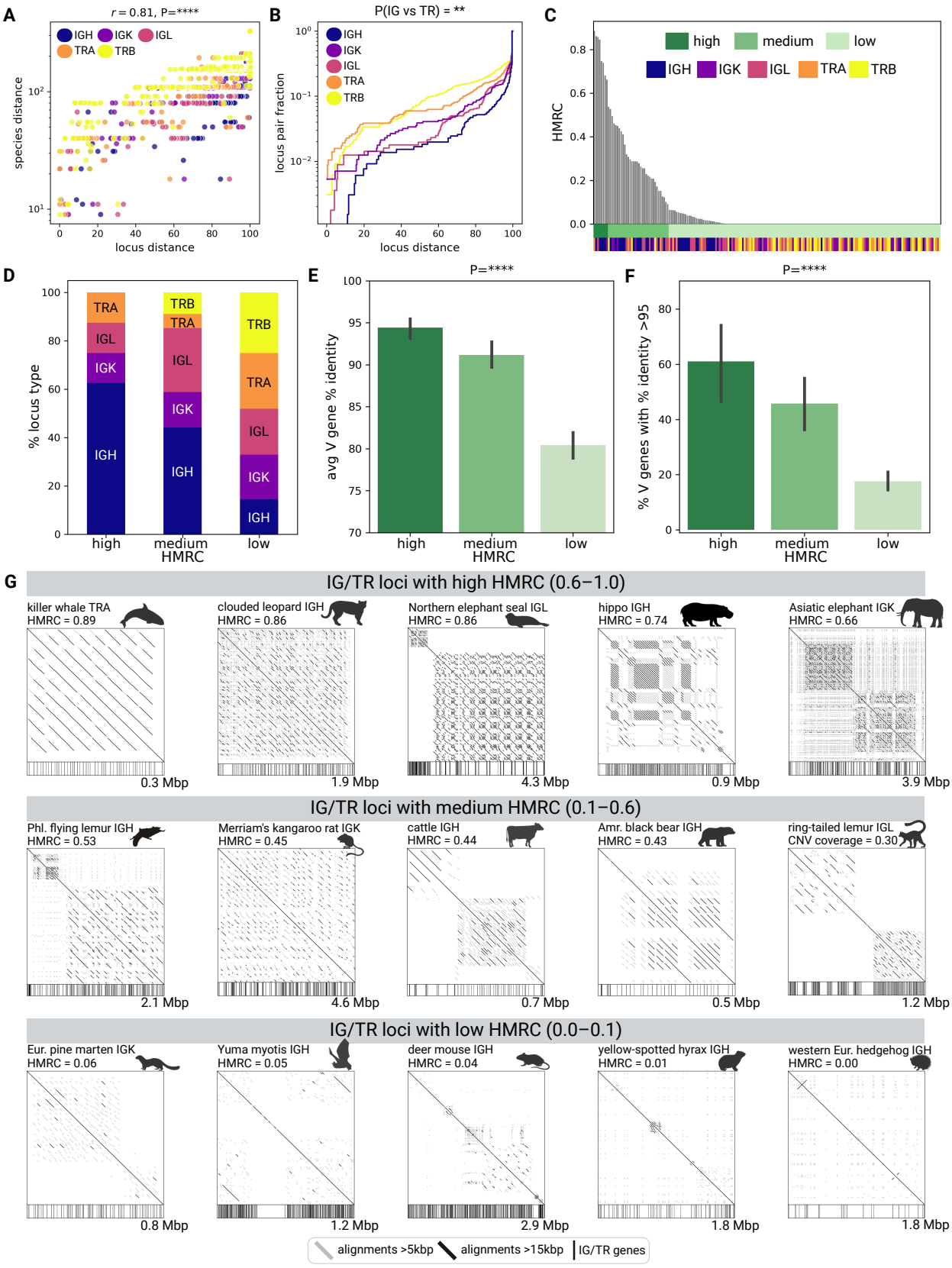
A
r = 0.81, P=****
IGH IGK IGL
TRA TRB
species distance
locus distance
B
P(IG vs TR) = **
IGH
IGK
IGL
TRA
TRB
locus pair fraction
locus distance
C
high medium low
IGH IGK IGL TRA TRB
HMRC
D
% locus type
high
medium
HMRC
low
E
P=****
avg V gene % identity
F
P=****
% V genes with % identity >95
G
IG/TR loci with high HMRC (0.6–1.0)
killer whale TRA
HMRC = 0.89
0.3 Mbp
clouded leopard IGH
HMRC = 0.86
1.9 Mbp
Northern elephant seal IGL
HMRC = 0.86
4.3 Mbp
hippo IGH
HMRC = 0.74
0.9 Mbp
Asiatic elephant IGK
HMRC = 0.66
3.9 Mbp
IG/TR loci with medium HMRC (0.1–0.6)
Phl. flying lemur IGH
HMRC = 0.53
2.1 Mbp
Merriam's kangaroo rat IGK
HMRC = 0.45
4.6 Mbp
cattle IGH
HMRC = 0.44
0.7 Mbp
Amr. black bear IGH
HMRC = 0.43
0.5 Mbp
ring-tailed lemur IGL
CNV coverage = 0.30
1.2 Mbp
IG/TR loci with low HMRC (0.0–0.1)
Eur. pine marten IGK
HMRC = 0.06
0.8 Mbp
Yuma myotis IGH
HMRC = 0.05
1.2 Mbp
deer mouse IGH
HMRC = 0.04
2.9 Mbp
yellow-spotted hyrax IGH
HMRC = 0.01
1.8 Mbp
western Eur. hedgehog IGH
HMRC = 0.00
1.8 Mbp
alignments >5kbp
alignments >15kbp
IG/TR genes

517

Figure 3. High multiplicity repeat content (HMRC) in IG/TR loci. (A) Locus distance vs species distance for all pairs of IG/TR loci of the same chain types. Points are colored according to the locus chain type: IGH (blue), IGK (purple), IGL (pink), TRA (orange), TRB (yellow). The species distances are shown in the logarithmic scale. Pearson's correlation and P-value are shown at the top of the plot. **(B)** The cumulative histograms of locus distance values for five chain types. **(C)** HMRC of IG/TR loci sorted in descending order of the values. Each bar is colored in shades of green according to the HMRC class: high (dark), medium (medium), low (pale) and chain type (colors are consistent with **A**). **(D)** Fraction of each locus type in each of three HMRC classes. **(E)** Average percent identity of productive V genes in IG/TR loci across three HMRC classes. **(F)** The fraction of productive V genes with at least 95% similarity to another V gene in the same locus across three HMRC classes. **(G)** Examples of IG/TR loci with high, medium, and low HMRC. Each locus is shown as a dot plot, alignments longer than 15 (5) kbp are shown in black (gray). Positions of IG/TR genes are shown along the bottom of each plot.

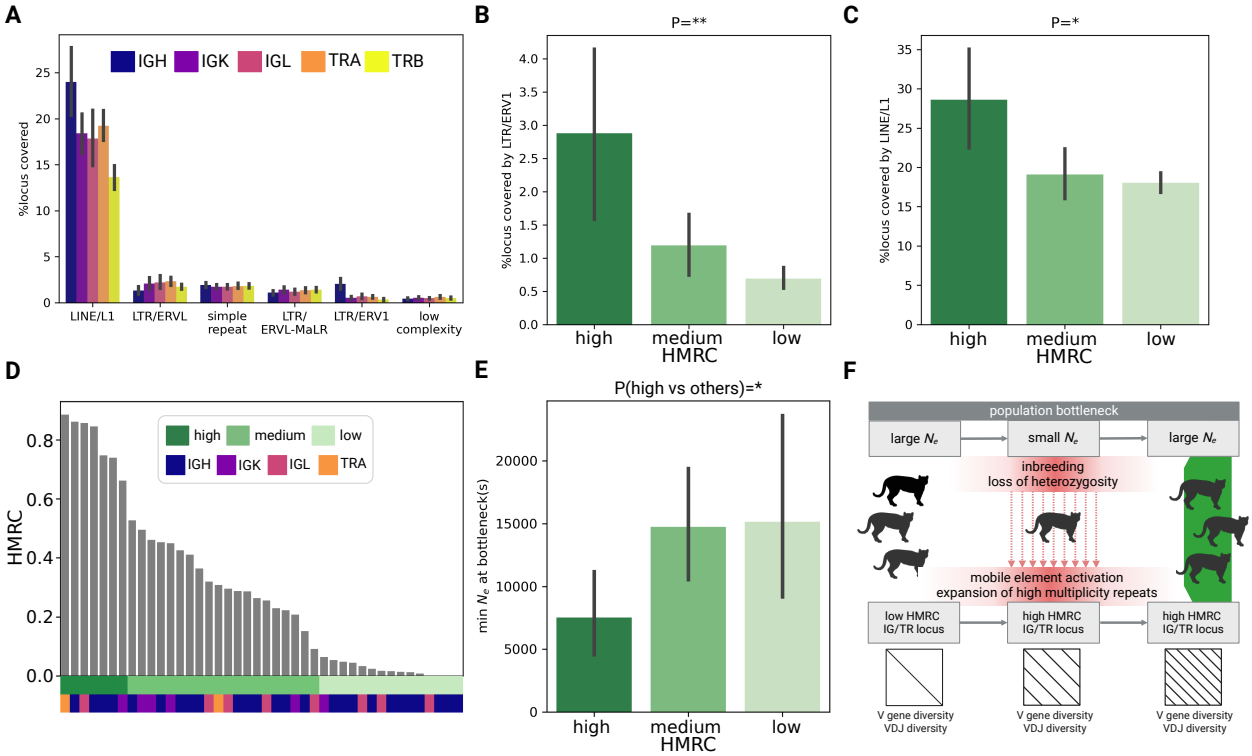

Figure 4. Characteristics of IG/TR loci with high, medium, and low HMRC. (A) Percentages of sequences covered by LINE/L1, LTR/ERVL, simple repeats, LTR/ERVL-MalR, LTR/ERV1, and low complexity repeats across five types of IG/TR loci. **(B)** Percentages of IG/TR loci covered by LTR/ERVL repeats across three HMRC classes. **(C)** Percentages of IG/TR loci covered by LINE/L1 repeats across three HMRC classes. **(D)** HMRC values (max HMRC value per species) sorted in descending order. Bars along the bottom show HMRC classes and the type of the corresponding locus. **(E)** The minimum N_e value during population bottlenecks across three HMRC classes for non-closely related species. **(F)** A hypothesis showing links between population bottlenecks, loss of heterozygosity, activation of mobile elements, and high multiplicity repeat expansion in IG/TR loci.

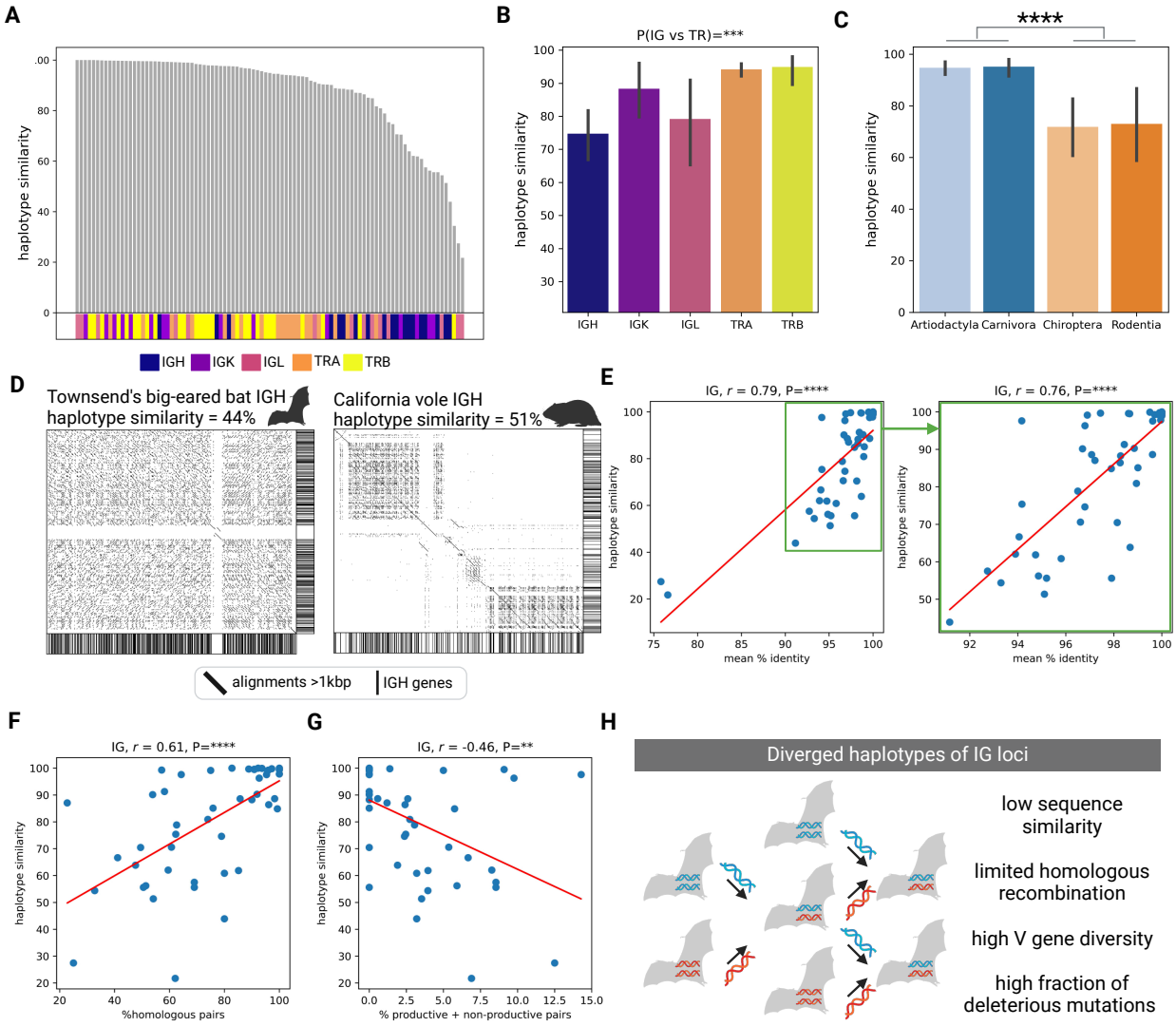

Figure 5. The variation of IG/TR locus haplotypes. (A) Haplotype similarities computed across 95 pairs of IG/TR haplotypes and sorted in descending order. The horizontal bar on the bottom shows IG/TR locus types. **(B)** Haplotype similarities across five types of IG/TR loci. P-value at the top shows differences between haplotype similarities values in IG and TR loci. **(C)** Haplotype similarities of IG haplotypes in four orders: Artiodactyla, Carnivora, Chiroptera, and Rodentia. P-value at the top corresponds to differences between combined Artiodactyla and Carnivora IG haplotype similarities vs combined Chiroptera and Rodentia IG haplotype similarities. **(D)** Dot plots of diverged haplotypes of Townsend's big-eared bat IGH locus (left) and the California vole IGH (right). Only alignments longer than 1 kbp are shown. Bars along the bottom and the right of each plot shows positions of IGH genes. **(E)** Haplotype similarity vs average V gene similarity in IG haplotypes across all haplotype pairs (left) and all haplotypes without two outliers in the lower left corner (right). Pearson's correlation and corresponding P-values are shown at the top of each plot here and further. **(F)** Haplotype similarity vs percentage of homologous V gene pairs across all IG haplotypes. **(G)** Haplotype similarity vs percentage of V gene pairs with one productive and

557 one non-productive gene across all IG haplotypes. **(H)** A hypothetical scenario resulting in highly
558 diverged IG haplotypes and their characteristics summarizing panels E-G.

559 # Tables

Order	Sample ID	Latin Name	Common Name	Haplotype1	Haplotype 2
Artiodactyla	mBalAcu1	*Balaenoptera acutorostrata*	Minke whale	GCA_949987535.1	GCA_950005055.1
Artiodactyla	mBosTau	*Bos taurus*	Cattle (Piedmontese)	10.5281/zenodo.5906579	
Artiodactyla	mOrcOrc1	*Orcinus orca*	Killer whale	GCA_937001465.1	GCA_937001455.1
Artiodactyla	mPhoSin1	*Phocoena sinus*	Vaquita	GCA_008692025.1	GCA_008692045.1
Artiodactyla	mCamDro1	*Camelus dromedarius*	Dromedary	genomeark.org/genomeark-all/Camelus_dromedarius.html	
Artiodactyla	mHipAmp2	*Hippopotamus amphibius kiboko*	Hippopotamus	GCA_030028035.1	GCF_030028045.1
Carnivora	mCanLor1	*Canis lupus orion*	Greenland wolf	GCA_905319855.2	GCA_905319845.1
Carnivora	mLutLut1	*Lutra lutra*	Eurasian river otter	GCA_902655055.2	GCA_902653095.1
Carnivora	mLynCan4	*Lynx canadensis*	Canada lynx	GCA_007474595.2	GCA_007474575.2
Carnivora	mMelMel3	*Meles meles*	European badger	GCA_922990625.1	GCA_922984935.2
Carnivora	mMusErm1	*Mustela erminea*	Stoat	GCA_009829155.1	GCA_009829165.1
Carnivora	mNeoNeb1	*Neofelis nebulosa*	Clouded leopard	GCA_028018385.1	GCA_028018655.1
Carnivora	mZalCal1	*Zalophus californianus*	California sea lion	GCA_009762305.2	GCA_009762295.2
Carnivora	mMarMar1	*Martes martes*	European pine marten	genomeark.org/vgp-all/Martes_martes.html	
Carnivora	mMusLut2	*Mustela lutreola*	European mink	genomeark.org/genomeark-all/Mustela_lutreola.html	
Carnivora	mPumCon1.1	*Puma concolor*	Mountain lion	GCA_028749985.3	GCA_028749965.3
Carnivora	mMusNiv1	*Mustela nivalis*	Least weasel	genomeark.org/genomeark-all/Mustela_nivalis.html	
Carnivora	mUrsAme1.0	*Ursus americanus*	American black bear	GCA_024610735.1	GCA_024610745.1
Carnivora	UrsArc2.0	*Ursus arctos*	Brown bear	GCF_023065955.2	NA
Carnivora	mLynRuf1	*Lynx rufus*	Bobcat	GCF_022079265.1	GCA_022079275.1
Carnivora	mMirAng1	*Mirounga angustirostris*	Northern elephant seal	GCA_029215605.1	GCA_029215635.1
Chiroptera	mMyoDau2	*Myotis daubentonii*	Daubenton's bat	genomeark.org/vgp-all/Myotis_daubentonii.html	
Chiroptera	mPleAur1	*Plecotus auritus*	Brown big-eared bat	genomeark.org/vgp-all/Plecotus_auritus.html	
Chiroptera	mEptNil1	*Eptesicus nilssonii*	Northern bat	genomeark.org/vgp-all/Eptesicus_nilssonii.html	
Chiroptera	mCorTow1.0	*Corynorhinus townsendii*	Townsend's big-eared bat	GCA_026230055.1	GCA_026230045.1
Chiroptera	mMyoYum1.0	*Myotis yumanensis*	Yuma myotis	GCA_028538775.1	GCA_028536395.1
Cingulata	mDasNov1	*Dasypus novemcinctus*	Nine-banded armadillo	genomeark.org/genomeark-all/Dasypus_novemcinctus.html	
Dermoptera	mCynVol1	*Cynocephalus volans*	Philippine flying lemur	GCA_027409185.1	GCA_027409165.1
Didelphimorphia	mMacEug1	*Macropus eugenii*	Tammar wallaby	GCA_028372415.1	GCA_028389975.1
Didelphimorphia	mMonDom1	*Monodelphis domestica*	Gray short-tailed opossum	GCA_027887165.1	GCA_027917375.1

Eulipotyphla	mSorAra2	*Sorex araneus*	Common shrew	GCA_027595985.1	GCA_027595995.1
Eulipotyphla	mEriEur2	*Erinaceus europaeus*	Western European hedgehog	GCA_950295315.1	GCA_950295305.1
Hyracoidea	mHetBru1	*Heterohyrax brucei*	Yellow-spotted hyrax	GCA_028571685.1	GCA_028571665.1
Perissodactyla	mDicBic1	*Diceros bicornis*	Black rhinoceros	GCA_020826845.1	GCA_020826835.1
Pholidota	mManPen7	*Manis pentadactyla*	Chinese pangolin	GCA_030020395.1	GCA_030020945.1
Primates	mLemCat1	*Lemur catta*	Ring-tailed lemur	GCA_020740605.1	GCA_020740595.1
Primates	mNycCou1	*Nycticebus coucang*	Slow loris	GCA_027406575.1	GCA_027406535.1
Proboscidea	mEleMax1	*Elephas maximus*	Asiatic elephant	GCA_024166365.1	GCA_024166345.1
Rodentia	mChiNiv1	*Chionomys nivalis*	European snow vole	GCA_950005125.1	GCA_950005115.1
Rodentia	mMusAve1	*Muscardinus avellanarius*	Hazel dormouse	genomeark.org/vgp-all/Muscardinus_avellanarius.html	
Rodentia	mPerMan1.0	*Peromyscus maniculatus*	Deer mouse	GCA_026167925.1	GCA_026167925.1
Rodentia	mThoBot1.0	*Thomomys bottae*	Botta's pocket gopher	GCA_024803745.1	GCA_024803775.1
Rodentia	mMicCal1.0	*Microtus californicus*	California vole	GCA_028537955.1	GCA_028537755.1
Rodentia	mDipMer1.0	*Dipodomys merriami*	Merriam's kangaroo Rat	GCA_024711535.1	GCA_024711525.1

Table 1. Species summary with accession numbers for assemblies.

561

Sample ID	Common species name	Locus with the highest HMRC	HMRC	HMRC class
mOrcOrc1	Killer whale	TRA	0.89	high
mNeoNeb1	Clouded leopard	IGH*	0.86	high
mMirAng1	Northern elephant seal	IGL	0.86	high
mPumCon1.1	Mountain lion	IGH*	0.84	high
mLynRuf1	Bobcat	IGH*	0.75	high
mHipAmp2	Hippopotamus	IGH	0.74	high
mEleMax1	Asiatic elephant	IGK	0.66	high
mCynVol1	Philippine flying lemur	IGH	0.53	medium
mManPen7	Chinese pangolin	IGK	0.50	medium
mDasNov1	Nine-banded armadillo	IGK	0.46	medium
mLynCan4	Canada lynx	IGH*	0.45	medium
mDipMer1.0	Merriam's kangaroo rat	IGK	0.45	medium
mBosTau	Cattle	IGH	0.44	medium
mUrsAme1.0	American black bear	IGH	0.43	medium
mPhoSin1	Vaquita	IGH*	0.41	medium
mBalAcu1	Minke whale	IGH*	0.36	medium
mCanLor1	Greenland wolf	IGL	0.32	medium
mChiNiv1	European snow vole	TRA	0.31	medium
mLemCat1	Ring-tailed lemur	IGL	0.30	medium
mMacEug1	Tammar wallaby	IGH	0.29	medium
mCamDro1	Dromedary	IGH	0.29	medium
mPleAur1	Brown big-eared bat	IGH	0.26	medium
mSorAra2	Common shrew	IGL	0.26	medium
mNycCou1	Slow loris	IGH	0.23	medium
mDicBic1	Black rhinoceros	IGH	0.22	medium
mThoBot1.0	Botta's pocket gopher	IGK	0.21	medium
mEptNil1	northern bat	IGH	0.15	medium
mCorTow1.0	Townsend's big-eared bat	IGL	0.09	medium
mMarMar1	European pine marten	IGK	0.06	low
mLutLut1	Eurasian river otter	IGH	0.05	low
mMyoYum1.0	Yuma myotis	IGH	0.05	low
mPerMan1.0	Deer mouse	IGH	0.04	low
mMusNiv1	Least weasel	IGL	0.03	low
mMyoDau2	Daubenton's bat	IGH	0.02	low
mMonDom1	Gray short-tailed opossum	IGL	0.02	low
mZalCal1	California sea lion	IGH	0.02	low
mMusLut2	European mink	IGH	0.01	low
mMelMel3	European badger	IGH	0.01	low

mHetBru1	Yellow-spotted hyrax	IGH	0.01	low
mMusErm1	Stoat	IGL	0.00	low
mMusAve1	Hazel dormouse	IGH	0.00	low
mMicCal1.0	California vole	IGH	0.00	low
mEriEur2	Western European hedgehog	IGH	0.00	low

562 **Table 2. Species with the maximum HMRC values across all five types of IG/TR loci.** The
563 corresponding locus and the selected HMRC value as well as the HMRC class are specified.
564 Three groups of closely related species were shown as rows colored in green (cetaceans), yellow
565 (felines), and blue (mustelids). For green and yellow groups, loci of the same type were selected.
566 The minimum N_e value of the brown bear was not computed because the genome assembly was
567 reported as haploid.
568

References

Alberts B, Johnson A, Lewis J, Raff M, Roberts K, Walter P. The generation of antibody diversity. InMolecular Biology of the Cell. 4th edition 2002. Garland Science.

Banach BB, Cerutti G, Fahad AS, Shen CH, De Souza MO, Katsamba PS, Tsybovsky Y, Wang P, Nair MS, Huang Y, Francino-Urdaniz IM. Paired heavy-and light-chain signatures contribute to potent SARS-CoV-2 neutralization in public antibody responses. Cell Reports. 2021 Oct 5;37(1).

Bratsch S, Wertz N, Chaloner K, Kunz TH, Butler JE. The little brown bat, M. lucifugus, displays a highly diverse VH, DH and JH repertoire but little evidence of somatic hypermutation. Developmental & Comparative Immunology. 2011 Apr 1;35(4):421-30.

Briney B, Inderbitzin A, Joyce C, Burton DR. Commonality despite exceptional diversity in the baseline human antibody repertoire. Nature. 2019 Feb 21;566(7744):393-7.

Chen N. Using Repeat Masker to identify repetitive elements in genomic sequences. Current protocols in bioinformatics. 2004 Mar;5(1):4-10.

Chen J, Lu L, Robb SM, Collin M, Okumoto Y, Stajich JE, Wessler SR. Genomic diversity generated by a transposable element burst in a rice recombinant inbred population. Proceedings of the National Academy of Sciences. 2020 Oct 20;117(42):26288-97.

Collins AM, Watson CT. Immunoglobulin light chain gene rearrangements, receptor editing and the development of a self-tolerant antibody repertoire. Frontiers in Immunology. 2018 Oct 8;9:2249.

Consuegra J, Gaffé J, Lenski RE, Hindré T, Barrick JE, Tenaillon O, Schneider D. Insertion-sequence-mediated mutations both promote and constrain evolvability during a long-term experiment with bacteria. Nature communications. 2021 Feb 12;12(1):980.

Danecek P, Bonfield JK, Liddle J, Marshall J, Ohan V, Pollard MO, Whitwham A, Keane T, McCarthy SA, Davies RM, Li H. Twelve years of SAMtools and BCFtools. Gigascience. 2021 Feb;10(2):giab008.

Das S, Hirano M, Tako R, McCallister C, Nikolaidis N. Evolutionary genomics of immunoglobulin-encoding loci in vertebrates. Current genomics. 2012 Apr 1;13(2):95-102.

De Kort H, Legrand S, Honnay O, Buckley J. Transposable elements maintain genome-wide heterozygosity in inbred populations. Nature Communications. 2022 Nov 17;13(1):7022.

DeKosky, B.J., Lungu, O.I., Park, D., Johnson, E.L., Charab, W., Chrysostomou, C., Kuroda, D., Ellington, A.D., Ippolito, G.C., Gray, J.J. and Georgiou, G., 2016. Large-scale sequence and

structural comparisons of human naive and antigen-experienced antibody repertoires. Proceedings of the National Academy of Sciences, 113(19), pp.E2636-E2645.

Drummond, A. J. and A. Rambaut. 2007. BEAST: Bayesian evolutionary analysis by sampling trees. BMC Evolutionary Biology 7:214.

Engelbrecht E, Rodriguez OL, Shields K, Schultze S, Tieri D, Jana U, Yaari G, Lees WD, Smith ML, Watson CT. Resolving haplotype variation and complex genetic architecture in the human immunoglobulin kappa chain locus in individuals of diverse ancestry. Genes & Immunity. 2024 Aug;25(4):297-306.

Freckleton RP, Harvey PH, Pagel M. Phylogenetic analysis and comparative data: a test and review of evidence. The American Naturalist. 2002 Dec;160(6):712-26.

Goel M, Sun H, Jiao WB, Schneeberger K. SyRI: finding genomic rearrangements and local sequence differences from whole-genome assemblies. Genome biology. 2019 Dec;20:1-3.

Hedges SB, Marin J, Suleski M, Paymer M, Kumar S. Tree of life reveals clock-like speciation and diversification. Molecular biology and evolution. 2015 Apr 1;32(4):835-45.

Jaffe DB, Shahi P, Adams BA, Chrisman AM, Finnegan PM, Raman N, Royall AE, Tsai F, Vollbrecht T, Reyes DS, Hepler NL. Functional antibodies exhibit light chain coherence. Nature. 2022 Nov 10;611(7935):352-7.

Janeway C, Travers P, Walport M, Shlomchik MJ. Immunobiology: the immune system in health and disease. New York, NY, USA: Garland Pub.; 2001 Apr 4.

Kaduk M, Corcoran M, Karlsson Hedestam GB. Addressing IGHV gene structural diversity enhances immunoglobulin repertoire analysis: lessons from rhesus macaque. Frontiers in immunology. 2022 Mar 28;13:818440.

Kos JT, Safonova Y, Shields KM, Silver CA, Lees WD, Collins AM, Watson CT. Characterization of extensive diversity in immunoglobulin light chain variable germline genes across biomedically important mouse strains. BioRxiv. 2022 May 1:2022-05.

Lam Si Tung Ho and Cécile Ané. A linear-time algorithm for Gaussian and non-Gaussian trait evolution models. Systematic Biology. 2014 Feb 04; 63(3):397-408.

Lefranc MP. Nomenclature of the human immunoglobulin kappa (IGK) genes. Experimental and clinical immunogenetics. 2001 Sep 6;18(3):161-74.

Li H. Aligning sequence reads, clone sequences and assembly contigs with BWA-MEM. arXiv preprint arXiv:1303.3997. 2013 Mar 16.

Li H. Minimap2: pairwise alignment for nucleotide sequences. Bioinformatics. 2018 Sep 15;34(18):3094-100.

Li H, Durbin R. Inference of human population history from individual whole-genome sequences. Nature. 2011 Jul 28;475(7357):493-6.

Li TT, Xia T, Wu JQ, Hong H, Sun ZL, Wang M, Ding FR, Wang J, Jiang S, Li J, Pan J. De novo genome assembly depicts the immune genomic characteristics of cattle. Nature Communications. 2023 Oct 19;14(1):6601.

Lin MJ, Langmead B, Safonova Y. IGLoo: Profiling the Immunoglobulin Heavy chain locus in Lymphoblastoid Cell Lines with PacBio High-Fidelity Sequencing reads. bioRxiv. 2024 Jul 23.

Luo S, Jane AY, Li H, Song YS. Worldwide genetic variation of the IGHV and TRBV immune receptor gene families in humans. Life science alliance. 2019 Apr 1;2(2).

Ma L, Liu L, Li J, Zhou H, Xiao J, Ma Q, Yao X. Landscape of IGH germline genes of Chiroptera and the pattern of Rhinolophus affinis bat IGH CDR3 repertoire. Microbiology Spectrum. 2024 Apr 2;12(4):e03762-23.

Martin J, Ponstingl H, Lefranc MP, Archer J, Sargan D, Bradley A. Comprehensive annotation and evolutionary insights into the canine (Canis lupus familiaris) antigen receptor loci. Immunogenetics. 2018 Apr;70:223-36.

Moya ND, Yan SM, McCoy RC, Andersen EC. The long and short of hyperdivergent regions. Trends in Genetics. 2024 Dec 19.

Noé L, Kucherov G. YASS: enhancing the sensitivity of DNA similarity search. Nucleic acids research. 2005 Jul 1;33(suppl_2):W540-3.

Pennell M, Rodriguez OL, Watson CT, Greiff V. The evolutionary and functional significance of germline immunoglobulin gene variation. Trends in immunology. 2023 Jan 1;44(1):7-21.

Peres A, Upadhyay AA, Klein V, Saha S, Rodriguez OL, Vanwinkle ZM, Karunakaran K, Metz A, Lauer W, Lin MC, Melton T. A Broad Survey and Functional Analysis of Immunoglobulin Loci Variation in Rhesus Macaques. bioRxiv. 2025 Jan 10:2025-01.

Pospelova M, Safonova Y. PatchWorkPlot: simultaneous visualization of local alignments across multiple sequences. arXiv preprint arXiv:2503.20766. 2025.

Pursell T, Reers A, Mikelov A, Kotagiri P, Ellison JA, Hutson CL, Boyd SD, Frank HK. Genetically and functionally distinct immunoglobulin heavy chain locus duplication in bats. bioRxiv. 2024 Aug 9:2024-08.

Ramesh A, Darko S, Hua A, Overman G, Ransier A, Francica JR, Trama A, Tomaras GD, Haynes BF, Douek DC, Kepler TB. Structure and diversity of the rhesus macaque immunoglobulin loci through multiple de novo genome assemblies. Frontiers in immunology. 2017 Oct 27;8:1407.

Raybould MI, Greenshields-Watson A, Agarwal P, Aguilar-Sanjuan B, Olsen TH, Turnbull OM, Quast NP, Deane CM. The Observed T Cell Receptor Space database enables paired-chain repertoire mining, coherence analysis, and language modeling. Cell Reports. 2024 Sep 24;43(9).

Revell, L. J. phytools 2.0: an updated R ecosystem for phylogenetic comparative methods (and other things). PeerJ. 2024. 12, e16505.

Rhie A, McCarthy SA, Fedrigo O, Damas J, Formenti G, Koren S, Uliano-Silva M, Chow W, Fungtammasan A, Kim J, Lee C. Towards complete and error-free genome assemblies of all vertebrate species. Nature. 2021 Apr 29;592(7856):737-46.

Robinson JT, Thorvaldsdóttir H, Winckler W, Guttman M, Lander ES, Getz G, Mesirov JP. Integrative genomics viewer. Nature biotechnology. 2011 Jan;29(1):24-6.

Rodriguez OL, Gibson WS, Parks T, Emery M, Powell J, Strahl M, Deikus G, Auckland K, Eichler EE, Marasco WA, Sebra R. A novel framework for characterizing genomic haplotype diversity in the human immunoglobulin heavy chain locus. Frontiers in immunology. 2020 Sep 23;11:2136.

Rodriguez OL, Safonova Y, Silver CA, Shields K, Gibson WS, Kos JT, Tieri D, Ke H, Jackson KJL, Boyd SD, Smith ML, Marasco WA, Watson CT. Genetic variation in the immunoglobulin heavy chain locus shapes the human antibody repertoire. Nat Commun. 2023;14(1):4419.

Safonova Y, Shin SB, Kramer L, Reecy J, Watson CT, Smith TP, Pevzner PA. Variations in antibody repertoires correlate with vaccine responses. Genome research. 2022 Apr 1;32(4):791-804.

Sampson JM, Miller RD. Evolution of the Structure and Organization of the Mammalian Immunoglobulin Loci. The Journal of Immunology. 2023 May;210(Supplement_1):224-01.

Schountz T, Baker ML, Butler J, Munster V. Immunological control of viral infections in bats and the emergence of viruses highly pathogenic to humans. Frontiers in immunology. 2017 Sep 11;8:1098.

Schroeder Jr HW. Similarity and divergence in the development and expression of the mouse and human antibody repertoires. Developmental & Comparative Immunology. 2006 Jan 1;30(1-2):119-35.

Sepulveda MA, Garrett FE, Price-Whelan A, Birshtein BK. Comparative analysis of human and mouse 3′ Igh regulatory regions identifies distinctive structural features. Molecular immunology. 2005 Mar 1;42(5):605-15.

Shaffer HB, Toffelmier E, Corbett-Detig RB, Escalona M, Erickson B, Fiedler P, Gold M, Harrigan RJ, Hodges S, Luckau TK, Miller C. Landscape genomics to enable conservation actions: the California Conservation Genomics Project. Journal of Heredity. 2022 Dec 1;113(6):577-88.

Sirupurapu V, Safonova Y, Pevzner PA. Gene prediction in the immunoglobulin loci. Genome research. 2022 Jun 1;32(6):1152-69.

Smith, T.P., Bickhart, D.M., Boichard, D., Chamberlain, A.J., Djikeng, A., Jiang, Y., Low, W.Y., Pausch, H., Demyda-Peyrás, S., Prendergast, J. and Schnabel, R.D., 2023. The Bovine Pangenome Consortium: democratizing production and accessibility of genome assemblies for global cattle breeds and other bovine species. Genome biology, 24(1), p.139.

Solyom S, Kazazian HH. Mobile elements in the human genome: implications for disease. Genome medicine. 2012 Feb;4:1-8.

Todesco M, Owens GL, Bercovich N, Légaré JS, Soudi S, Burge DO, Huang K, Ostevik KL, Drummond EB, Imerovski I, Lande K. Massive haplotypes underlie ecotypic differentiation in sunflowers. Nature. 2020 Aug 27;584(7822):602-7.

Tonegawa S. Somatic generation of antibody diversity. Nature. 1983 Apr 14;302(5909):575-81.

Uyeda JC, Zenil-Ferguson R, Pennell MW. Rethinking phylogenetic comparative methods. Systematic Biology. 2018 Nov 1;67(6):1091-109.

Upham NS, Esselstyn JA, Jetz W. Inferring the mammal tree: species-level sets of phylogenies for questions in ecology, evolution, and conservation. PLoS biology. 2019 Dec 4;17(12):e3000494.

Wang F, Ekiert DC, Ahmad I, Yu W, Zhang Y, Bazirgan O, Torkamani A, Raudsepp T, Mwangi W, Criscitiello MF, Wilson IA. Reshaping antibody diversity. Cell. 2013 Jun 6;153(6):1379-93.

Watson CT, Steinberg KM, Huddleston J, Warren RL, Malig M, Schein J, Willsey AJ, Joy JB, Scott JK, Graves TA, Wilson RK. Complete haplotype sequence of the human immunoglobulin heavy-chain variable, diversity, and joining genes and characterization of allelic and copy-number variation. The American Journal of Human Genetics. 2013 Apr 4;92(4):530-46.

Watson CT, Kos JT, Gibson WS, Newman L, Deikus G, Busse CE, Smith ML, Jackson KJ, Collins AM. A comparison of immunoglobulin IGHV, IGHD and IGHJ genes in wild-derived and classical inbred mouse strains. Immunology and cell biology. 2019 Nov;97(10):888-901.

Wertz N, Vazquez J, Wells K, Sun J, Butler JE. Antibody repertoire development in fetal and neonatal piglets. XII. Three IGLV genes comprise 70% of the pre-immune repertoire and there is little junctional diversity. Molecular immunology. 2013 Oct 1;55(3-4):319-28.

Xie KT, Wang G, Thompson AC, Wucherpfennig JI, Reimchen TE, MacColl AD, Schluter D, Bell MA, Vasquez KM, Kingsley DM. DNA fragility in the parallel evolution of pelvic reduction in stickleback fish. Science. 2019 Jan 4;363(6422):81-4.

Yoo D, Rhie A, Hebbar P, Antonacci F, Logsdon GA, Solar SJ, Antipov D, Pickett BD, Safonova Y, Montinaro F, Luo Y. Complete sequencing of ape genomes. BioRxiv. 2024 Oct 5.

Zhang W, Dasmahapatra KK, Mallet J, Moreira GR, Kronforst MR. Genome-wide introgression among distantly related Heliconius butterfly species. Genome biology. 2016 Dec;17:1-5.

Zhu Y, Watson C, Safonova Y, Pennell M, Bankevich A. Assessing assembly errors in immunoglobulin loci: a comprehensive evaluation of long-read genome assemblies across vertebrates. bioRxiv. 2024 Aug 2.